



Kinetic study of reaction $C_2H_5 + HO_2$ in a photolysis reactor with time-resolved Faraday rotation spectroscopy

Hongtao Zhong ^a, Chao Yan ^{a,*}, Chu C. Teng ^b, Guoming Ma ^a,
Gerard Wysocki ^b, Yiguang Ju ^a

^a Department of Mechanical and Aerospace Engineering, Princeton University, Princeton, NJ 08544, USA

^b Department of Electrical Engineering, Princeton University, Princeton, NJ 08544, USA

Received 7 November 2019; accepted 13 July 2020

Available online 14 October 2020

Abstract

The rate constant and branching ratios of ethyl reaction with hydroperoxy radical, $C_2H_5 + HO_2$ (1), a key radical-radical reaction for intermediate temperature combustion chemistry, were measured *in situ* for the first time in a photolysis Herriott cell by using mid-IR Faraday rotation spectroscopy (FRS) and UV-IR direct absorption spectroscopy (DAS). The microsecond time-resolved diagnostic technique in this work enabled the direct rate measurements of the target reaction at 40 and 80 mbar and reduced the experimental uncertainty considerably. C_2H_5 and HO_2 radicals were generated by the photolysis of $(COCl)_2/C_2H_5I/CH_3OH/O_2/He$ mixture at 266 nm. By direct measurements of the transient profiles of C_2H_5 , HO_2 and OH concentrations, the overall rate constant for this reaction at 297 K was determined as $k_1(40 \text{ mbar}) = (3.8 \pm 0.8) \times 10^{-11} \text{ cm}^3 \text{ molecule}^{-1} \text{ s}^{-1}$ and $k_1(80 \text{ mbar}) = (4.1 \pm 1.0) \times 10^{-11} \text{ cm}^3 \text{ molecule}^{-1} \text{ s}^{-1}$. The direct observation of hydroxyl radical (OH) indicated that OH formation channel was the major channel with a branching ratio of 0.8 ± 0.1.

© 2020 The Combustion Institute. Published by Elsevier Inc. All rights reserved.

Keywords: Radical-radical reaction; Hydroperoxy radical; Faraday rotation spectroscopy; Chemical kinetics; Rate constant

1. Introduction

Reactions involving hydroperoxy radicals, HO_2 , are known to play a critical role in the chain-branching processes of low and intermediate temperature fuel oxidation processes such as cool flames [1], warm flames [2], and engine knocking [3,4], especially at elevated pressures [5]. However,

HO_2 reaction kinetics is difficult to study due to lacking of direct photolysis source and multiple reaction channels with different product reactivities. Determination of not only the reaction rate but also the branching ratios of the different channels are critical to improve the predictability of kinetic models. Taking one of the simplest examples, the reaction between HO_2 and C_2H_5 , the possible reactions channels from Wu et al. [6] with thermochemistry data at 298 K taken from Ref. [7,8] (in kcal mol⁻¹) are

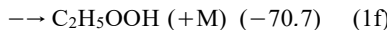
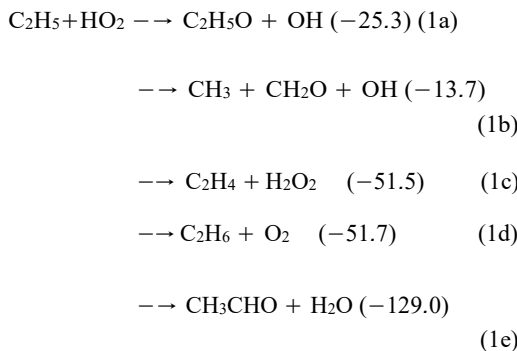
* Corresponding author.

E-mail address: chaoy@princeton.edu (C. Yan).

Table 1

Summary of reported rate constant values for reaction $\text{C}_2\text{H}_5 + \text{HO}_2$ at room temperature.

reaction	$k / \times 10^{-11} \text{ cm}^3 \text{ molecule}^{-1} \text{ s}^{-1}$	Method	P /mbar	Ref
1	3.81 ± 0.84	IR FRS + UV-IR DAS	40	this work
1	4.08 ± 1.05	IR FRS + UV-IR DAS	80	this work
1, 1a	5.15 ± 1.66	Time-resolved Mass Spectrometry	1.2	[9]
1c	0.30 ± 0.01	Mass Spectrometry	10^{-3}	[12]
1a	4.98	QRRK Theory Estimation	10	[11]
1	6.88	VTST + RRKM theory		[6]
1b	4	Estimation		[10]
1c	0.05	Estimation		[10]
1d	0.05	Estimation		[10]



Channel 1a has been considered as a major chain propagation channel [9–11]. A possible decomposition of $\text{C}_2\text{H}_5\text{O}$ radicals may further result in another radical CH_3 and an active intermediate species CH_2O (1b) with a large energy barrier [6]. On the other hand, three chain-termination channels as (1c–1e) will lead to stable molecules.

Despite the significance of the reaction between hydroperoxy radical with ethyl radicals (1a - 1f), little experimental data are available. Table 1 summarizes the currently available kinetic information of the rate constant k_1 as well as the experimental and theoretical methods including this work. The earliest estimation by Tsang and Hampson in 1980s [10] expected OH formation channel (1b) to be the major channel with an estimated rate constant $k = 4 \times 10^{-11} \text{ cm}^3 \text{ molecule}^{-1} \text{ s}^{-1}$. The first related theoretical prediction performed by Bozzelli and Dean [11] assumed channel (1a) as a fast HO_2 consumption pathway with $k = 4.98 \times 10^{-11} \text{ cm}^3 \text{ molecule}^{-1} \text{ s}^{-1}$. Dobis and Benson [12] were the first to determine the rate constant of channel (1c) by mass spectrometry in the reaction system of $\text{C}_2\text{H}_6/\text{O}_2/\text{Cl}_2$ under millitorr pressure. By using a steady-state treatment of a complex reaction mechanism, they extracted the rate constant from the observed concentrations of HO_2 and H_2O_2 . Unfortunately, the products of the previously assumed main channel (1a), $\text{C}_2\text{H}_5\text{O}$, could not be

detected in their experiments. Ludwig et al. [9] in 2006 measured the overall rate constant of $\text{C}_2\text{H}_5 + \text{HO}_2$ reaction by measuring HO_2 and C_2H_5 concentration-time profiles using the pulsed-laser photolysis time-resolved mass spectrometry (PLP-MS) experimental technique at 1.2 mbar. They observed mass signals of $\text{C}_2\text{H}_5\text{O}$ ($\text{C}_2\text{H}_3\text{O}$ fragment), indicating that channel (1a) was the major reaction channel. However, the PLP-MS method was limited to pressure around 1 mbar. Moreover, the nozzle sampling in the mass spectrometry method caused concerns of radical quenching, especially at low pressures. Most recently, Wu et al. [6] investigated this reaction theoretically by applying high level quantum chemistry computations in conjunction with variational transition-state theory (VTST) and Rice–Ramsperger–Kassel–Marcus (RRKM) theory over wide temperature and pressure ranges ($T = 220 – 3000 \text{ K}$; $P = 1 \times 10^{-4} – 100 \text{ bar}$). They found that the products as $\text{C}_2\text{H}_5\text{O}$ and OH became the primary products at lower pressures or higher temperatures. The predicted branching ratios of reaction (1a) varies from 0.96 at $1 \times 10^{-4} \text{ bar}$ to 0.66 at 100 bar.

Nevertheless, contradictory results were reported by the only two existing experimental determinations as seen in Table 1. Moreover, experimental conditions were limited to low pressures. Higher pressure kinetic data is needed for practical combustion systems. Recent advances in UV-IR direct absorption spectroscopy (DAS) and Faraday rotation spectroscopy (FRS) make it possible to perform *in situ* measurements at higher pressure with microsecond time resolution. UV-DAS has been applied to study the kinetics of a similar reaction $\text{CH}_3 + \text{HO}_2$ in the shock tube [13] and slow-flow pulsed-laser photolysis reactor [14]. However, the measurement uncertainty is large due to spectrum interference. Other sensitive absorption techniques including near-IR cavity ring-down spectroscopy (CRDS) [15] may not be suitable for the current kinetic measurements as the ringdown time limits the time resolution and further causes diffusion issue. In this work, we increased the time resolution of HO_2 measurements to $2.5 \mu\text{s}$ by fast line-scanned FRS (discussed in Section 2.2), with which we were able to resolve the prompt HO_2 formation in the

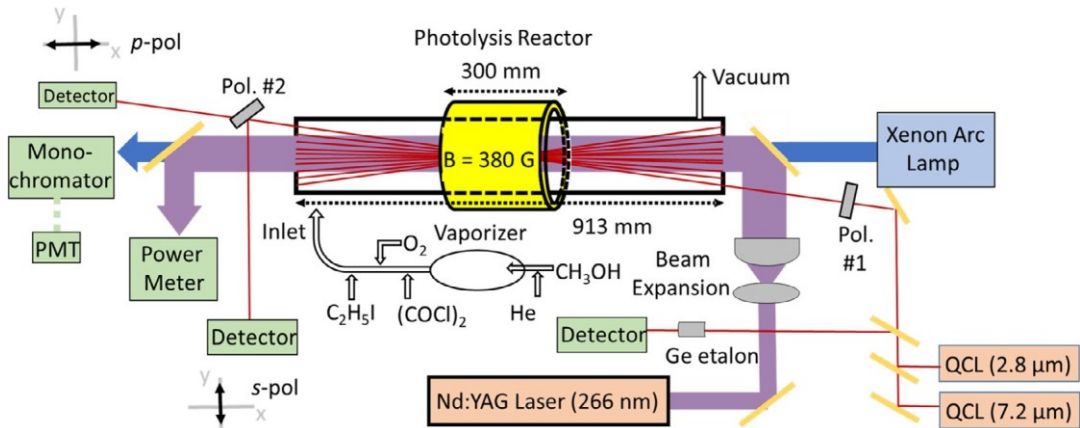


Fig. 1. Experimental apparatus of the slow-flow photolysis reactor and diagnostic system.

initial microsecond time scale and further reduced the experimental uncertainty for the rate constants of the target reaction.

FRS is a highly selective and sensitive dispersion-based magneto-optical detection only for paramagnetic species. Over the past decades, FRS was successfully applied in detecting important species including HO_2 [16], OH [17], and NO_x [18] due to its promising immunity from spectral interference of non-paramagnetic species. However, to date due to the low signal to noise ratio, the time resolution of line-scanned FRS HO_2 diagnostics was limited to 100 μs [16]. Significant increase of FRS time-resolution for HO_2 diagnostics is needed for the study of $\text{HO}_2 + \text{C}_2\text{H}_5$ reaction kinetics as the reaction sensitivity for the measured species decays sharply after the initial 50 μs (discussed in Section 3.3).

The goal of this work is to directly measure the rate constant and the branching ratios of C_2H_5 and HO_2 reaction at room temperature ($T = 297 \text{ K}$) and 40 and 80 mbar He pressure by applying microsecond time-resolved *in situ* FRS and DAS diagnostic method. We photolyzed the mixture of $\text{C}_2\text{H}_5\text{I}/(\text{COCl})_2/\text{CH}_3\text{OH}/\text{O}_2/\text{He}$ at 266 nm. Temporal profiles of C_2H_5 , OH and HO_2 radicals were recorded via transient UV-DAS signals at 220 nm, IR-DAS signals at 2.8 μm , and IR-FRS signals at 7.2 μm , respectively. By fitting the time-resolved experimental data with a small reaction mechanism, the rate constant of $\text{C}_2\text{H}_5 + \text{HO}_2$ was determined as shown in Table 1. The major reaction channel is also discussed.

2. Experimental section

2.1. Experimental setup

The experimental apparatus has been reported in previous studies [16,19,20]. Therefore, only

a short description for the current setup is given here. The schematic diagram is shown in Fig. 1.

Nd:YAG laser photolysis was coupled with UV-IR DAS and IR-FRS in a multipass Herriott cell. The reactor was made of a 913 mm long, 50 mm i.d. quartz tubing. At both ends of the reactor, a pair of gold-coated spherical mirrors (250 mm focal length) on CaF_2 substrate were installed to form a 21-pass configuration. The uncoated central part of the spherical mirrors allowed for the Nd:YAG laser photolysis beam (Quanlet Q-smart 850, 266 nm) to pass through the reactor cell and generate spatially homogeneous concentrations of radicals inside the cell. The laser energy output was *ca.* 140 mJ/pulse. The laser beam was expanded by a pair of convex lenses. At the entrance of the reactor, the laser beam was passed through 22 mm i.d. apertures to ensure the uniformity of the light intensity, while at the exit of the reactor, the laser photon fluence was monitored by high-energy pyroelectric sensors (Ophir, PE50BF-DIF-C). The quantification of absolute photon flux in the reactor will be discussed in Section 2.3. The Nd:YAG laser was operated at a repetition rate of 0.4 Hz to satisfy slow-flow conditions and ensure the entire replacement of the gas volume between laser pulses.

The gases He (99.999 %) and O_2 (99.5 %, Airgas) were used as supplied. Methanol (99.9 %, Fisher Scientific) was delivered by a syringe pump (KdScientific, Legato 110) through a central capillary tube (200 μm) into a pre-vaporization chamber with a flow rate of 0.02–0.05 ml/min. $(\text{COCl})_2$ (99.9 %) and $\text{C}_2\text{H}_5\text{I}$ (99.9 %, Sigma-Aldrich) were degassed prior to use by repeated freeze-pump-thaw cycles. They were prepared in a glass mixing system and then mixed thoroughly with helium in a stainless steel cylinder before experiment. The gas flows were regulated by calibrated mass flow controllers (MKS instruments).

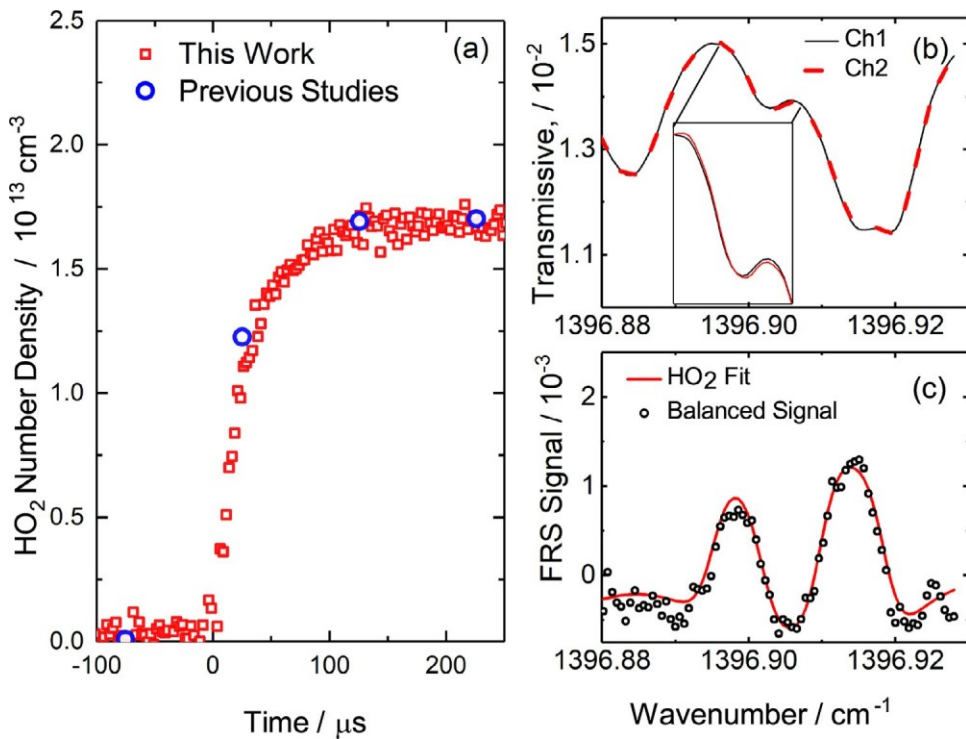


Fig. 2. (a) Balanced FRS detection of HO₂ under different time resolutions. Previous work [16]: 100 μ s. This work: 2.5 μ s (b) Measured transmission from two channels after digital balancing. Inset zooms into the region with HO₂ FRS signal. (c) A sample FRS spectrum of HO₂ due to Faraday rotation in the presence of 380 G magnetic field. HO₂ concentration was quantified as 1.3×10^{13} molecule cm⁻³ (13.5 ppmv).

2.2. Line-scanned FRS

The time-resolved FRS signals of HO₂ radicals were measured at the spectral region around 1396.91 cm⁻¹ (7.2 μ m) using a quantum cascade laser (QCL) from Thorlabs. The targeted HO₂ line at 1396.90 cm⁻¹ is a Q-branch spectral feature and corresponds to a vibrational transition. To perform FRS, a 300 mm long solenoid with DC current was placed to generate a nearly uniform magnetic field (*ca.* 380 G) around the reactor. After accounting for 21 passes, the effective optical path length within the solenoid was *ca.* 6.3 m. A pair of wire grid polarizers (labeled as Pol. #1 and #2 in Fig. 1) were located before and after the multi-pass cell. Pol. #2 was adjusted to 45° with respect to the incident polarization angle and the exit beam was divided into orthogonal polarization components (measured as p-polarization and s-polarization), each of which was detected by a photodetector (VIGO, PVI-4TE-8). The differential signal between p-polarization and s-polarization with proper digital balancing was directly related to the Faraday rotation signals shown in Fig. 2(c), revealing the onset of the photolysis event and the subsequent kinetics of HO₂.

At each photolysis event, the recording time window spanned 7 ms and was triggered 2 ms before the photolysis pulse. The HO₂ profiles at the first 200 μ s after the laser pulse are shown in Fig. 2(a). Sawtooth signals were applied to trigger the current ramping and therefore the QCL frequency ramping around 7.2 μ m. The time resolution of HO₂ profiles at each photolysis event was directly related to QCL ramping frequency and the sampling rate of the data acquisition device (Razor Digitizer). By increasing the time resolution from 100 μ s reported in previous literature [16] to 2.5 μ s, we were capable of fully resolving the HO₂ formation profiles (shown in Fig. 2(a)), which was essential for the rate constant measurements (See further discussion in Section 3.3). However, the fast ramping also caused the distortion of sawtooth signals and therefore insufficient data points to construct a spectrum at every scan, leading to increased detection limit. The chosen time resolution (2.5 - 4 μ s) was thus a compromise between sufficient resolution for target reaction and promising sensitivity. The current setup provided 6.8×10^{11} molecule cm⁻³ (0.7 ppm) sensitivity to HO₂ with averaging over 100 photolysis events. Fig. 2(b) shows the directly measured

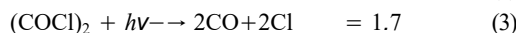
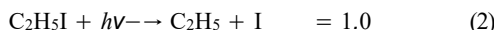
transmission around 7.2 μm , where absorption lines of methanol are clearly visible. However, this spectral interference was effectively suppressed in the FRS signal as shown in Fig 2(c), where HO₂ signal was clear and we applied least mean square fitting using HITRAN line parameters to determine the concentration.

2.3. In situ actinometry

In situ actinometry based on the ozone depletion with detailed reaction mechanism and well-characterized cross-section of ozone at wavelength of 253.65 nm (mercury line) was applied to quantify the photon flux inside the reactor. Details of this technique can be found elsewhere [14,19]. In this work we monitored the ozone in the photolysis of O₃/O₂/He mixtures at 80 mbar and 297 K. Photon fluence F (photons cm^{-2}) per laser pulse was determined by fitting the experimental temporal profiles of O₃ with numerical simulations from a small reaction mechanism. During the measurements of C₂H₅+HO₂ kinetics, the readout of the pyroelectric detector measuring the laser pulse energy after the reactor was recorded and then used to introduce proper corrections for the drift of the photon fluence. The daily actinometry experiments were provided before and after the experiments. During the whole set of kinetic measurements, the photon fluence was $(1.88 \pm 0.27) \times 10^{16}$ photons/ cm^2/pulse .

2.4. Radical generation and monitoring

The generation and monitoring of radical species are critical for kinetic studies of radical-radical reactions. In this work, the radicals C₂H₅ and HO₂ were generated by Nd:YAG laser photolysis (266 nm) of mixtures containing (COCl)₂, CH₃OH, O₂ and C₂H₅I. Photolysis of (COCl)₂ and C₂H₅I yields the primary products Cl and C₂H₅ according to



The quantum yields and the absorption cross sections, σ ((COCl)₂) 1.7×10^{-19} $\text{cm}^2 \text{molecule}^{-1}$ and σ (C₂H₅I) 1.1×10^{-18} $\text{cm}^2 \text{molecule}^{-1}$, were reported previously [21,22]. The primary radicals from reaction (3) were then converted rapidly into secondary radicals HO₂ via the H atom abstraction reactions as [23]



The experimental conditions are summarized in Table 2. The concentrations of the precursors used were $(0.53\text{--}2.10) \times 10^{15}$ molecule cm^{-3} for C₂H₅I, $(2.81\text{--}3.22) \times 10^{15}$ molecule cm^{-3} for (COCl)₂,

$(8.02\text{--}9.30) \times 10^{15}$ molecule cm^{-3} for CH₃OH, and $(4.23\text{--}4.91) \times 10^{15}$ molecule cm^{-3} for O₂. The peak radical concentrations of generated HO₂ and C₂H₅ for typical kinetic runs were $(0.80\text{--}1.60) \times 10^{13}$ molecule cm^{-3} and $(1.02\text{--}2.86) \times 10^{13}$ molecule cm^{-3} .

HO₂ radicals were monitored by FRS (discussed in Section 2.2). C₂H₅ and OH were monitored by UV-IR DAS. A DFB-QCL from Nanoplus (DFB-260290) was used to target Q(1.5e) and Q(1.5f) transitions of the ²T_{3/2} electronic state of OH radicals around 3568.52 cm^{-1} (2.8 μm). The effective path length was *ca.* 7.5 m for IR-DAS OH measurements. The absorption cross section of OH was calibrated using H₂O/O₂/O₃/He mixtures (discussed in our previous study [19]). The decay of C₂H₅ radicals was monitored by absorption at 220 nm (2400 groove/mm grating, 300 mm focal distance, both slits 0.25 mm, triangle slit function, FWHM=0.76 nm) using a 75 W (Oriel) short arc xenon lamp combined with an imaging spectrometer (Acton 2500i) and a photo-multiplier tube (Hamamatsu R7154).

3. Results and discussions

3.1. Calibrations of absolute radical concentrations

The absolute radical concentrations of C₂H₅ and HO₂ are critical for radical-radical kinetic studies. We applied different calibration methods for the absolute number densities of measured C₂H₅, HO₂, and OH. Photolysis of gas mixtures of CH₃OH/O₂/(COCl)₂/He was applied to calibrate the HO₂ FRS signals at 7.2 μm following the reaction (3–5). Fig 3(a) depicts a sample time-resolved FRS signals at 40 mbar as an example. The comparison of the numerically simulated HO₂ concentration-time profiles with the experimentally-measured FRS signals showed good agreement. Photolysis of gas mixtures of C₂H₅I/He was used to calibrate the C₂H₅ DAS signals at 220 nm. A sample time-resolved profile of C₂H₅ is shown in Fig. 3(b), where the well-characterized C₂H₅ self-decay reaction rate constant was taken from Ref. [24]. Photolysis of gas mixtures of H₂O/O₂/O₃/He was used to calibrate the OH DAS signals at 2.8 μm . OH was generated by O₃ $h\nu$ O(¹D), O₂ and Q(¹D) + H₂O → 2OH. The calibrated OH cross section was 3.1×10^{-18} $\text{cm}^2 \text{molecule}^{-1}$. The details can be found in previous studies [19].

3.2. Rate measurements for the reaction C₂H₅ + HO₂

The overall rate constant of the radical-radical reaction C₂H₅ + HO₂ → products was measured at room temperature (T=297 K) and 40 and 80 mbar reaction pressures. Sample FRS profiles are shown in Fig. 4. The small reaction mechanism

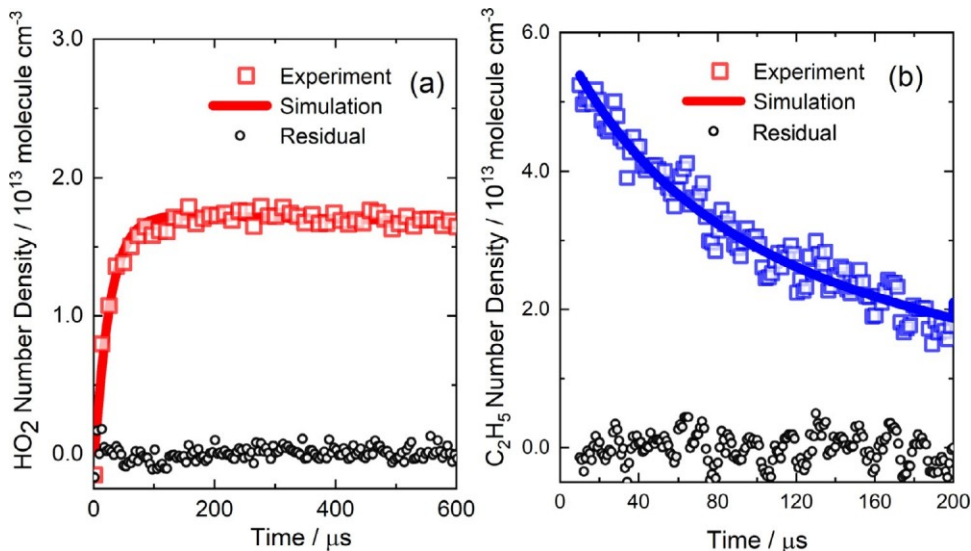


Fig. 3. (a) HO₂ concentration-time profile measured by IR-FRS at 7.2 μm with numerical fitting. (Reaction condition No. 1 in Table 2) (b) C₂H₅ self-decay time history measured by UV-DAS at 220 nm with numerical fitting. (Reaction condition No. 5 in Table 2).

Table 2

Experimental conditions and results. $T \geq 297$ K. All concentrations are given in units of molecule cm^{-3} and the rate constants in molecule $^{-1} \text{cm}^3 \text{s}^{-1}$.

No	P / mbar	$[\text{O}_2]_0 / 10^{15}$	$[\text{CH}_3\text{OH}]_0 / 10^{15}$	$[(\text{COCl})_2]_0 / 10^{15}$	$[\text{C}_2\text{H}_5\text{I}]_0 / 10^{15}$	$[\text{Cl}]_0 / 10^{13}$	$[\text{C}_2\text{H}_5]_0 / 10^{13}$	$k_1 / 10^{-11}$
1	40	4.59	8.69	2.97	0.00	1.94	0.00	—
2	40	4.51	8.55	2.93	0.53	1.74	1.20	2.88
3	40	4.39	8.31	2.84	1.06	1.50	2.13	4.02
4	40	4.30	8.16	2.79	1.58	1.32	2.86	4.53
5	40	0.00	0.00	0.00	1.92	0.00	6.57	—
6	40	4.11	7.78	2.73	1.45	2.01	2.70	3.80
7	80	5.02	9.51	3.25	0.00	1.75	0.00	—
8	80	4.91	9.30	3.18	0.58	1.48	1.02	3.19
9	80	4.79	9.08	3.11	1.16	1.30	1.85	5.25
10	80	4.69	8.88	3.04	1.72	1.12	2.41	3.81
11	80	0.00	0.00	0.00	2.10	0.00	3.98	—
12	80	4.69	8.88	3.11	1.76	1.14	2.33	4.00

was built in this study for simulation and fitting experimental data to determine the rate constant and branching ratios for the target reaction (See details in the Supplementary Material). The measured FRS profiles were fitted by numerical solutions of a system of differential equations corresponding to the reaction mechanism using Micro-math Scientist [25].

At each experimental condition, five different time-resolved profiles were recorded: (i, ii) transient HO₂ FRS profiles and C₂H₅ UV absorption profiles were obtained by the photolysis of mixtures of CH₃OH/O₂/(COCl)₂/He and C₂H₅I/He, respectively. The experiments (i, ii), which were free from contributions of the target reaction, were used to examine the absolute HO₂

and C₂H₅ radical concentrations. (iii) HO₂ profiles were recorded by photolysis of mixtures of CH₃OH/O₂/(COCl)₂/C₂H₅I/He. This set of experimental data was used to determine the rate constant of the target reaction. (iv) While transient absorption profiles at 220 nm were also recorded, the measured UV-DAS signals at 220 nm are strongly contaminated by other species as C₂H₅O₂ and HO₂ and therefore it is extremely difficult to obtain clean C₂H₅ signals. (v) Time-resolved profiles of OH were used to determine the major channel of the target reaction. In order to quantify the absolute concentration of radicals, *in situ* actinometry measurements were performed before and after the kinetic experiments. In addition, the experiments (i, ii) were carried out before any kinetic measure-

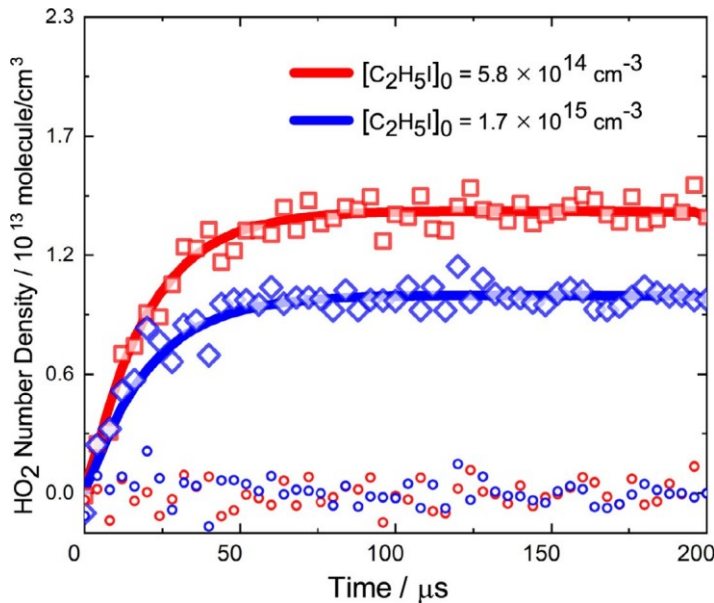


Fig. 4. HO_2 concentration-time profile measured by IR-FRS at $7.2 \mu\text{m}$ with numerical fitting under different concentrations of C_2H_5 . (Red rectangular points refer to reaction condition No. 8 and blue diamond points refer to reaction condition No. 10 in Table 2). (For interpretation of the references to color in this figure legend, the reader is referred to the web version of this article.)

ments such that appropriate HO_2 and C_2H_5 reference profiles were valid.

The transient FRS profiles of HO_2 were fitted by the reaction mechanism presented in the Supplementary Material. The fitting parameter was the overall rate constant of the target reaction. Good agreement between experimental data and fitting results within the experimental errors is shown in Fig. 4.

The results indicated that the rate constant of the target reaction was close to the high pressure limit under the current experimental conditions. The overall rate constant together with the standard deviation error bars is shown in Fig. 6. The results are close to (25 % lower) the most recently experimental determination by Ludwig et al. [9]. The small discrepancy is within the experimental uncertainty. Compared with the first experimental results reported by Dobis and Benson [12], our rate constant is higher by one order of magnitude. Since Dobis and Benson's experiments were performed in the millitorr pressure regime, their measurements might be within the falloff region.

3.3. Reaction pathway analysis

Two major factors contributing to the errors in this kinetic study are the uncertainty of the photon fluence inside the reactor (discussed in Section 2.3)

and the reaction mechanism. Therefore, it is important to evaluate the reaction mechanism.

Photolysis of precursors was prompt compared with all other chemical reactions. Therefore, they were treated separately in the reaction mechanism. Cl atoms and C_2H_5 radicals produced by photolysis of precursors initialized the subsequent reactions in the mechanism. The transient species in the kinetic modeling were C_2H_5 , Cl , HO_2 , OH , $\text{C}_2\text{H}_5\text{O}_2$, I , $\text{C}_2\text{H}_5\text{O}$, O , H , H_2O_2 , O_3 , CH_2OH . The concentrations of CH_3OH , $\text{C}_2\text{H}_5\text{I}$, O_2 were considered as constant since they were in large excess over transient species. The diffusion of HO_2 was also considered since the target rate constant was determined from the transient profiles of HO_2 .

Reaction pathway analysis of the reaction mechanism was carried out using the experimental conditions listed in the Table 2. Figure 6 displays the reaction rate-time profiles of the dominant consumption pathways for HO_2 radicals. It was clear that the target reaction dominated the fate of HO_2 radicals at the initial $150 \mu\text{s}$, which made the determination of k_1 from HO_2 concentration-time profiles possible.

The situation was different in the case of C_2H_5 radical profiles. Large amount of O_2 was introduced into the reaction system to generate sufficient HO_2 radicals. As a consequence, C_2H_5 radicals were consumed in a short period of time through the reaction $\text{C}_2\text{H}_5 + \text{O}_2 \rightarrow \text{C}_2\text{H}_5\text{O}_2$. The typical lifetime of C_2H_5 radicals is less than $200 \mu\text{s}$,

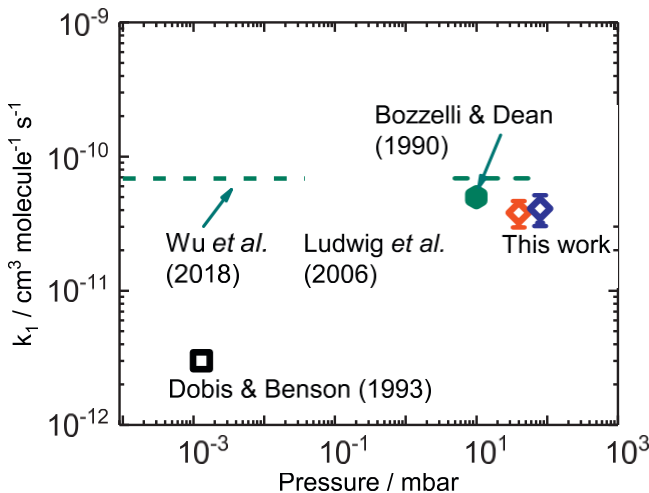


Fig. 5. Experimental measurements and theoretical predictions of reaction rate constants k_1 at different pressures and room temperature.

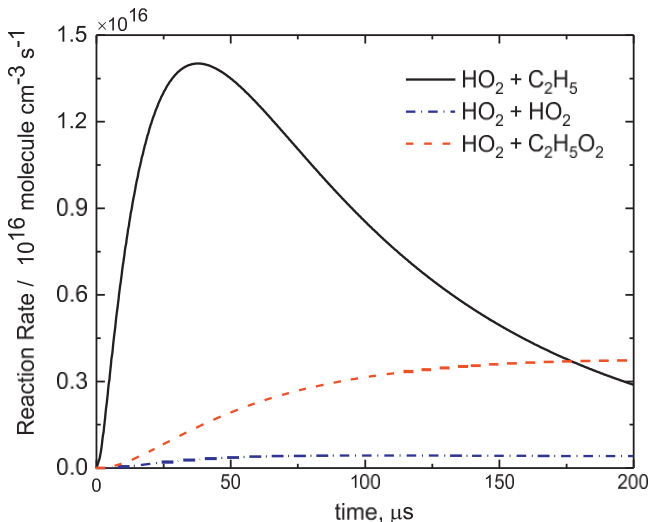


Fig. 6. Time evolution of reaction rates for dominant reactions of HO_2 calculated by the reaction mechanism.(Reaction condition No. 6 in Table. 2).

while the lifetime of HO_2 radicals is over 20 ms. Due to this large reaction time scale difference, we could only carefully control the radical generation so that the rising time of HO_2 radicals and the half life of C_2H_5 were similar ($\sim 50 \mu\text{s}$). In addition, great effort was made to increase the concentrations of C_2H_5 and therefore improve the sensitivity of the target reaction in terms of HO_2 radicals. The dominant reaction pathways for C_2H_5 are displayed in the Supplementary Material. As stated in the previous section, the absorption of C_2H_5 radical at wavelength 220 nm was interfered by HO_2 and $\text{C}_2\text{H}_5\text{O}_2$, which made it more difficult to deter-

mine the rate constant by using transient profiles at 220 nm.

3.4. Reaction branching ratio

The transient absorption profiles of OH radical at *ca.* 2.8 μm were fitted by the same reaction mechanism to determine the branching ratio, $(k_{1a} + k_{1b})/k_1$, of the target reaction as shown in Fig. 7(a). Fig. 7(b) shows the major reaction pathways for OH radicals. This *in situ* measurements of OH radicals directly indicated that OH formation was dominant. The branching ratio determined at

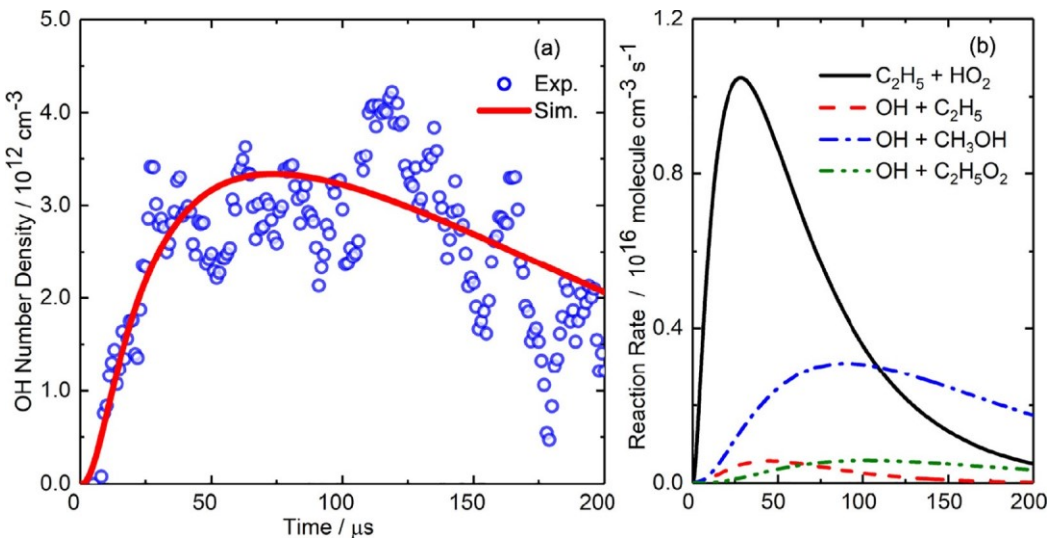


Fig. 7. (a) OH concentration-time profile measured by IR-DAS at $2.8 \mu\text{m}$ with numerical fitting (Reaction condition No. 6 in Table 2) (b) Time evolution of reaction rates for dominant reactions of OH calculated by the in-house kinetic model.

room temperature ($T = 297 \text{ K}$) and two reaction pressures ($p = 40$ and 80 mbar) is the following: $(k_{1a} + k_{1b})/k_1 = 0.8 \pm 0.1 \pm$

This measured branching ratio was slightly lower than values provided by the most recent experimental and theoretical determinations and in contrast with the original recommendation of Dobis and Benson [12], which proposed channel (1c) as the major channel.

4. Conclusions

The overall rate constant of the radical-radical reaction $\text{C}_2\text{H}_5 + \text{HO}_2$ was measured *in situ* for the first time at $T = 297 \text{ K}$ reaction temperature and $p = 40$ and 80 mbar pressure. HO_2 and C_2H_5 radicals with controlled concentrations were generated by 266 nm photolysis of mixtures of CH_3OH , O_2 , $\text{C}_2\text{H}_5\text{I}$ and $(\text{COCl})_2$ in He. We measured transient profiles of HO_2 with line-scanned FRS, C_2H_5 with UV-DAS, and OH with IR-DAS. Observed differences of HO_2 signals within the initial $200 \mu\text{s}$ with different $\text{C}_2\text{H}_5\text{I}$ concentrations could be attributed mainly to the influence of the target reaction. The overall uncertainty of the rate determination was reduced compared with previous studies. The evaluation based on a comprehensive reaction mechanism resulted in a total rate constant value at room temperature of $(3.8 \pm 0.8) \times 10^{-11} \text{ cm}^3 \text{ molecule}^{-1} \text{ s}^{-1}$ at 40 mbar , and $(4.1 \pm 1.0) \times 10^{-11} \text{ cm}^3 \text{ molecule}^{-1} \text{ s}^{-1}$ at 80 mbar . OH DAS signals revealed that OH-formation channel (1a–1b) was the major channel with a branching ratio of 0.80 ± 0.1 . This study contributes to an improved understanding of the kinetic coupling in

low and intermediate temperature fuel oxidation processes.

Declaration of Competing Interest

None.

Acknowledgments

This work was supported by NSF grants CBET 1903362 and 1507358. We acknowledge Dr. Stephen J. Klippenstein for helpful discussions.

Supplementary material

Supplementary material associated with this article can be found, in the online version, at doi:10.1016/j.proci.2020.07.095.

References

- [1] Y. Ju, C.B. Reuter, O.R. Yehia, T.I. Farouk, S.H. Won, Prog. Energy Combust. Sci. 75 (2019) 100787, doi:10.1016/j.pecs.2019.100787.
- [2] O.R. Yehia, C.B. Reuter, Y. Ju, Combust. Flame 195 (2018) 63–74.
- [3] W.R. Leppard, Combust. Sci. Technol. 43 (1-2) (1985) 1–20.
- [4] J. Cowart, J. Keck, J. Heywood, C. Westbrook, W. Pitz, Proc. Combust. Inst. 23 (1) (1991) 1055–1062.
- [5] F. Battin-Leclerc, Prog. Energy Combust. Sci. 34 (4) (2008) 440–498.

- [6] N.N. Wu, M.Z. Zhang, S.L. Ou-Yang, L. Li, *Molecules* 23 (8) (2018) 1919, doi:10.3390/molecules23081919.
- [7] B. Rusecic, R.E. Pinzon, M.L. Morton, G. von Laszewski, S.J. Bittner, S.G. Nijssure, K.A. Amin, M. Minkoff, A.F. Wagner, *J. Phys. Chem. A* 108 (45) (2004) 9979–9997.
- [8] J.M. Simmie, G. Black, H.J. Curran, J.P. Hinde, *J. Phys. Chem. A* 112 (22) (2008) 5010–5016.
- [9] W. Ludwig, B. Brandt, G. Friedrichs, F. Temps, *J. Phys. Chem. A* 110 (9) (2006) 3330–3337, doi:10.1021/jp0557464.
- [10] W. Tsang, R. Hampson, *J. Phys. Chem. Ref. Data* 15 (3) (1986) 1087–1279.
- [11] J.W. Bozzelli, A.M. Dean, *J. Phys. Chem.* 94 (8) (1990) 3313–3317, doi:10.1021/j100371a021.
- [12] O. Dobis, S.W. Benson, *J. Am. Chem. Soc.* 115 (19) (1993) 8798–8809, doi:10.1021/ja00072a038.
- [13] Z. Hong, D.F. Davidson, K.Y. Lam, R.K. Hanson, *Combust. Flame* 159 (10) (2012) 3007–3013, doi:10.1016/j.combustflame.2012.04.009.
- [14] M. Sangwan, L.N. Krasnoperov, *J. Phys. Chem. A* 117(14)(2013)2916–2923, doi:10.1021/jp4000889.
- [15] J. Thiebaud, C. Fittschen, *Appl. Phys. B* 85 (2-3) (2006) 383–389.
- [16] C.C. Teng, C. Yan, A. Rousso, T. Chen, Y. Ju, G. Wysocki, *CLEO* (2018) ATh3P-1.
- [17]
- [18] W. Zhao, G. Wysocki, W. Chen, E. Fertein, D. Le Coq, D. Petitprez, W. Zhang, *Opt. Express* 19 (3) (2011) 2493–2501.
- [19] K. Liu, R. Lewicki, F.K. Tittel, *Sens. Actuators, B* 237 (2016) 887–893.
- [20] C. Yan, C.C. Teng, T. Chen, H. Zhong, A. Rousso, H. Zhao, G. Ma, G. Wysocki, Y. Ju, *Combust. Flame* 212 (2020) 135–141.
- [21] H. Zhong, C. Yan, C.C. Teng, T. Chen, A.C. Rousso, G. Wysocki, Y. Ju, *AIAA Scitech 2019 Forum* (2019) 2065.
- [22] A.V. Baklanov, L.N. Krasnoperov, *J. Phys. Chem. A* 105 (1) (2001) 97–103.
- [23] J. Burkholder, S. Sander, J. Abbatt, J. Barker, R. Huie, C. Kolb, M. Kurylo, V. Orkin, D. Wilmouth, P. Wine, Chemical kinetics and photochemical data for use in atmospheric studies: evaluation number 18, *Technical Report*, Pasadena, CA: Jet Propulsion Laboratory, NASA, 2015.
- [24] C.A. Taatjes, D.B. Oh, *Appl. Opt.* 36 (24) (1997) 5817–5821.
- [25] S.J. Klippenstein, Y. Georgievskii, L.B. Harding, *Phys. Chem. Chem. Phys.* 8 (10) (2006) 1133–1147.
- [26] Micromath-Scientist, Inc., *Experimental Data Fitting, Microsoft Windows, Version 2* (1995).